HHS Public Access

Author manuscript

NMR Biomed. Author manuscript; available in PMC 2018 January 11.

Published in final edited form as:

NMR Biomed. 2017 October ; 30(10): . doi:10.1002/nbm.3758.

MRI reveals increased tumorigenesis following high fat feeding in a mouse model of triple-negative breast cancer

Devkumar Mustafi[1], **Sully Fernandez**[2], **Erica Markiewicz**[1], **Xiaobing Fan**[1], **Marta Zamora**[1], **Jeffrey Mueller**[3], **Matthew J. Brady**[2], **Suzanne D. Conzen**[4], and **Gregory S. Karczmar**[1]

[1]Department of Radiology, The University of Chicago, Chicago, Illinois 60637, USA

[2]Department of Medicine, Section of Adult and Pediatric Endocrinology, Diabetes and Metabolism, The University of Chicago, Chicago, Illinois 60637, USA

[3]Department of Pathology, The University of Chicago, Chicago, Illinois 60637, USA

[4]Department of Medicine, Section of Hematology and Oncology, The University of Chicago, Chicago, Illinois 60637, USA

Abstract

High animal fat consumption is associated with an increase in triple-negative breast cancer (TNBC) risk. Based on previous MRI studies demonstrating the feasibility of detecting very early non-palpable mammary cancers in simian virus 40 large T antigen (SV40TAg) mice, we examined the effect of dietary fat fed from weaning to young adulthood in this model of TNBC. Virgin female C3(1)SV40TAg mice ($n = 16$) were weaned at 3–4 weeks of age and then fed either a low fat diet (LFD) ($n = 8$, 3.7 kcal/g; 17.2% kcal from vegetable oil) or a high animal fat diet (HAFD) ($n = 8$, 5.3 kcal/g; 60% kcal from lard). After 8 weeks on the diet (12 weeks of age), fast spin echo MR images of inguinal mammary glands were acquired at 9.4 T. Following *in vivo* MRI, mice were sacrificed and inguinal mammary glands were excised and formalin fixed for *ex vivo* MRI. 3D volume-rendered MR images were then correlated with mammary gland histology to assess the glandular parenchyma and tumor burden. Using *in vivo* MRI, an average of 3.88 ± 1.03 tumors were detected per HAFD-fed mouse compared with an average of 1.25 ± 1.16 per LFD-fed mouse ($p < 0.007$). Additionally, the average tumor volume was significantly higher following HAFD feeding (0.53 ± 0.45 mm^3) compared with LFD feeding (0.20 ± 0.08 mm^3, $p < 0.02$). Analysis of *ex vivo* MR and histology images demonstrated that HAFD mouse mammary glands had denser parenchyma, irregular and enlarged ducts, dilated blood vessels, increased white adipose tissue, and increased tumor invasion. MRI and histological studies of the SV40TAg mice demonstrated that HAFD feeding also resulted in higher cancer incidence and larger mammary tumors. Unlike other imaging methods for assessing environmental effects on mammary cancer growth, MRI allows routine serial measurements and reliable detection of small cancers as well as accurate tumor volume measurements and assessment of the three-dimensional distribution of tumors over time.

Correspondence: Gregory S. Karczmar, Department of Radiology, The University of Chicago, Chicago, Illinois 60637, USA., gskarczm@uchicago.edu.

Keywords

high animal fat diet (HAFD); mouse mammary cancers; MRI histopathological correlation; triple-negative breast cancer (TNBC)

1 | INTRODUCTION

Breast cancer is the most commonly diagnosed malignancy among women in the United States and other Western countries; it remains the second leading cause of cancer mortality worldwide.[1,2] Epidemiological studies suggest an increase in the risk of triple-negative breast cancer (TNBC) in association with a high animal fat diet (HAFD).[3–8] Although there is a statistically significant association between obesity and cancer risk, there is little clinical information about how diet composition influences female breast development, breast fat physiology, and corresponding cancer subtype risk independent of weight gain. Long term dietary intervention studies with recently diagnosed breast cancer survivors show better prognosis and survival with reductions in fat intake in women with hormone receptor negative breast cancer,[9,10] but there is little information about how the HAFD influences the progression of pre-neoplastic and *in situ* cancers in the breast. Progression of pre-invasive neoplasms to invasive cancers is difficult to study in patients, as these early lesions are typically resected after diagnosis. As a result, use of an HAFD in animal models can provide important insights into early diet-induced changes in mammary gland biology and provide better insight intoTNBC progression. In addition, these studies of animal models could guide the development of preventive therapies.

The simian virus 40 large T antigen (SV40TAg) transgenic mouse model appears to recapitulate many of the phenotypic and genotypic characteristics of human TNBC.[11–13] Previous studies have shown that the consumption of a high fat diet does not significantly increase body weight in this model, but does shorten mammary tumor latency.[14] Therefore, this model makes it possible to directly study diet-induced effects on mammary gland biology independent of the confounding secondary effects of systemic changes that occur in generalized obesity. High fat feeding also increased mammary cancer growth rate in these mice, as qualitatively estimated by external palpation,[6,7] which limits detection to early tumors and does not provide accurate tumor volume and distribution measurements. In this study, the development of alterations to mammary ductal structures as well as formation of pre-palpable tumors was therefore studied by MRI in the SV40TAg mouse model.

Due to their inability to provide precise soft tissue imaging, computed tomography and ultrasound have not been adequate to monitor neoplastic changes during early stage mammary cancer progression in mice.[15,16] On the other hand, MRI provides excellent soft tissue contrast, can detect early cancer *in vivo* much more reliably than other imaging modalities, allows evaluation of the surrounding parenchyma, and allows accurate tumor volume measurements over time. Previous work from our laboratory demonstrated that *in vivo* T_2-weighted MRI reliably detects very early *in situ* mammary tumors in SV40TAg mice with high sensitivity and specificity, and differentiates *in situ* from invasive cancer.[17–20] Precise correlations between *in vivo* MR and histology images have also been

demonstrated.[20] Furthermore, serial MRI directly demonstrated great heterogeneity in initiation time, growth rate, and time at which *in situ* cancers became invasive.[21]

The goal of the present study was to determine whether dietary fat alters the incidence of mammary cancer in SV40TAg mice fed an HAFD from weaning. Using *in vivo* MRI and *ex vivo* MRI with excised glands analyzed histologically, here we report the early tumor incidence and tumor burden in SV40TAg mice fed an HAFD compared with those fed a low fat diet (LFD).

2 | MATERIALS AND METHODS

2.1 | Ethical statement

This study was carried out in strict accordance with the recommendations in the Guide for the Care and Use of Laboratory Animals of the National Institutes of Health. All animal work was approved by the University of Chicago Institutional Animal Care and Use Committee (IACUC). All efforts were made to minimize any suffering and mice were humanely euthanized following the experiments.

2.2 | Animals and diet

Sixteen FVB/N female mice homozygous for the SV40 TAg transgene were weaned at 3 weeks of age as previously described.[22] At 4 weeks of age, mice were separated and randomly assigned to either an LFD group ($n = 8$, 3.7 kcal/g; 17.2% kcal from vegetable oil) or an HAFD group ($n = 8$, 5.3 kcal/g; 60% kcal from lard). These diets were purchased from Harlan Laboratories (Madison, WI, USA).[23] Four female mice were housed together per diet group; cage food intake and individual body weight were monitored weekly. Table 1 provides a list of nutrients and ingredients for LFD- and HAFD-fed mice. After following these diets for 8 weeks, all 16 mice received MR scans at 12 weeks of age. Mice were anesthetized prior to *in vivo* MR imaging, and anesthesia was maintained during imaging with 1–2% isoflurane. Temperature, heart rate, and respiration rate were monitored with equipment from SA Instruments (Stony Brook, NY, USA), and the respiration was used to gate imaging. Following *in vivo* MRI studies at 12 weeks of age, mice were sacrificed by an overdose of isoflurane and cervical dislocation. Mammary tissues were then excised so that both *in situ* and invasive cancers detected by MRI could be correlated with histology.

2.3 | Preparation of mammary glands for *ex vivo* MRI and histology

After *in vivo* MRI studies, the mammary glands, while still connected to the skin, were excised from the mouse body and placed in 10% formalin for tissue fixation for two weeks. Prior to *ex vivo* imaging the skin was removed from formalin and rinsed daily with phosphate-buffered saline (Fisher Scientific, Waltham, MA, USA) for 3 days. The right inguinal gland from each mouse was chosen for *ex vivo* MRI and histology. The selected gland was then excised from the skin and placed between two layers of pathology foam, mimicking the exact position of the *ex vivo* mammary gland on the skin, and the exact position of the mammary gland in hematoxylin and eosin (H&E)-stained slices, as previously described.[20] Since the *ex vivo* gland was scanned by MRI in the same orientation

as the H&E-stained tissue, the *ex vivo* MR images served as a 'bridge' between *in vivo* MRI and histology to facilitate accurate correlation.

2.4 | MRI experiments

2.4.1 | *In vivo* imaging—MR images were acquired on a 9.4 T small animal scanner (Bruker, Billerica, MA, USA) with 11.6 cm inner diameter, actively shielded gradient coils (maximum constant gradient strength for all axes: 230 mT/m) using a 30 mm diameter quadrature mouse volume coil (Rapid MR International, Columbus, OH, USA). Multi-slice RARE (rapid acquisition with relaxation enhancement) T_2-weighted images with fat suppression were acquired with the following parameters: $T_R/T_{Eeffective}$ = 4000/20 ms, field of view (FOV) = 25.6 mm × 25.6 mm, matrix size = 256^2, slice thickness = 0.5 mm, RARE factor = 4, number of excitations (N_{EX}) = 2. In-plane resolution was 100 μm. For the inguinal glands (left and right), two interleaved sets of images were acquired to cover the slice gaps of 1 mm and then combined together for a total of 62 slices.

2.4.2 | *Ex vivo* imaging—*Ex vivo*** MR images were acquired on the same 9.4 T scanner. The wrapped, single mammary gland prepared as described above was placed in a homebuilt eight-leg, low pass, half-open birdcage coil (length = 3 cm, width = 3 cm, height = 2 cm). *Ex vivo* 3D images were acquired with the RARE T_2-weighted sequence with fat suppression and with $T_R/T_{Eeffective}$ = 4000/25 ms, FOV = 30 mm × 25 mm × 5 mm, matrix size = 384 × 320 × 64, isotropic resolution = 78 μm, and N_{EX} = 4.

2.5 | Histology

Following *ex vivo* MRI studies, an intact, right inguinal gland from each mouse was placed in a histology cassette and paraffin embedded. Typical tissue dimensions were 15 mm in length, 10 mm in width, and about 1.5 mm in thickness. About 20 H&E slices were sectioned from the 1.5 mm thick slice of tissue, as described previously.[20] Histological slides were then evaluated by an experienced breast pathologist (J.M.) and tissue was classified as normal gland, *in situ*, or invasive cancer.

2.6 | Data analysis

MRI data were processed and analyzed quantitatively using software written in IDL (Exelis VIS, Boulder, CO, USA). High resolution *ex vivo* MR images were used to facilitate correlation of *in vivo* images with histology. An integrated software program, Amira (FEI Visualization Sciences Group, Burlington, MA, USA), was used for volume rendering and 3D visualization of *in vivo* images as demonstrated previously.[20] Identification was confirmed by two observers—one (D.M.) with 10 years of experience in MRI and one (E.M.) with 10 years of experience in mouse histology. The person who classified the cancers as *in situ* or invasive cancer based on MRI was blinded to histopathology assessments.

Based on the sizes of *in situ* (150 to 400 μm in largest diameter) and invasive cancers (>400 μm in largest diameter) and their signal intensities on T_2-weighted MR images of 1.4 times that of muscle and of 2.3 times that of muscle, *in situ* cancers and invasive cancers, respectively, were accurately identified on *in vivo* MRI.[20] In the work presented here, *all*

invasive cancers identified on *in vivo* MRI in the entire inguinal gland were correlated with the corresponding cancers identified on histology. Using IDL, regions of interest (ROIs) for individual invasive tumors were drawn on every MR slice in which the tumor was detected. Each tumor was given a numerical label and the volume from each tumor's ROIs combined was calculated in mm^3. *In situ* cancers were also counted using the IDL software. Because *in situ* cancer is difficult to count throughout the entire mouse gland, four slices were chosen per mouse: two on the right-hand side of the mouse and two on the left-hand side. The first and second slices chosen were located three slices prior to the first slice of the left and right lymph node, respectively. The third and fourth slices that were chosen were located three slices after the last slices of the left and right lymph node were seen, respectively. Individual ductal carcinomas *in situ* (DCISs) per chosen slice were individually counted and then combined as a total for that mouse. Student's *t*-tests were performed for statistical analysis. A *p*-value less than 0.05 was considered significant.

3 | RESULTS

3.1 | Mammary ductal structures are altered following high animal fat feeding from weaning

Following weaning, SV40TAg female mice were fed either an LFD or an HAFD for 8 weeks. Mice given an HAFD did not gain significantly more weight than the LFD-fed mice (average body weight of 18.20 ± 1.04 g on LFD, compared with an average body weight of 19.75 ± 2.02 g on HAFD, $p < 0.075$). The FVB/N mouse strain was chosen for these studies since the females are resistant to high fat diet-induced obesity.[14] This allows for the direct assessment of the HAFD on the mammary gland, while avoiding the confounding factors of systemic hyperinsulinemia/hyperleptinemia arising from whole body weight gain and metabolic dysfunction. Analysis of axial T_2-weighted central MR images of mammary glands of mice fed LFD (Figure 1A) versus HAFD (Figure 1B) showed few areas of DCIS and darker mammary glands in the LFD mice. A brighter signal from parenchyma and more DCIS was found in HAFD mice. HAFD mice also show thicker and irregular ductal structure (Figure 1B), suggestive of more active mammary ducts as well as of abnormal ductal development.

3.2 | Fat composition and mammary gland structure in high resolution *ex vivo* MR images

Higher spatial resolution (isotropic resolution of 78 μm), 3D volume-rendered, *ex vivo* MR images of LFD- and HAFD-fed SV40TAg mouse mammary glands at 12 weeks of age (Figure 2) further illustrate the diet-induced changes to the mammary glands of these mice. Figure 2A, B shows *ex vivo* MR images with lymph nodes and invasive cancers indicated and labeled. Although the fat-suppressed fast spin echo sequence was used in each case (Figure 2), residual fat was still visible in HAFD-fed mouse glands due to the incomplete suppression of mammary fat (Figure 2B), indicating that the fat resonance was complex and contained multiple fat chemical shifts.[24]

Figure 2C, D shows color MR images of the mammary gland, comparing small areas as indicated by boxes in Figure 2A, B. A central slice containing the lymph node is seen in each image. The larger blue area in Figure 2D is due to denser parenchyma of the mice fed HAFD, and was produced with the same intensity criterion (thresholding) as used for the

lymph nodes in 2C, D. The color images in Figure 2C, D show much thicker and irregular ductal architecture in HAFD mouse mammary gland compared with LFD mouse mammary gland. Additionally, more branching points of mammary ducts were seen in the HAFD mice, suggesting altered ductal tree development, as indicated in Figure 2D.

3.3 | Increased tumor size in mice fed a high fat diet

Because of the very large number of *in situ* cancers throughout the entire mouse gland, four slices were chosen per mouse in each diet group as described in the 'Materials and methods' section. $n = 90$ *in situ* cancers were found in four slices of both glands of the LFD group ($n = 8$ mice) and $n = 130$ were found in the HAFD group ($n = 8$ mice). A plot (Figure 3) comparing the incidence of invasive cancers as a function of tumor volume in LFD and HAFD SV40TAg mice shows distinct differences between the two groups. Tumors found in the inguinal glands of both 12-week-old LFD and HAFD groups ($n = 8$ mice per group) were classified as either *in situ* or invasive based on the size and the relative signal intensity with respect to muscle and confirmed by histology, as previously described.[20]

As shown in Figure 3, we defined four groups by tumor volume. The number of tumors with volumes larger than 0.16 mm^3 was significantly greater in mice fed with HAFD compared with LFD-fed mice ($p < 0.007$). Differences in tumor incidence increased dramatically as tumor size increased (Figure 3). Differences in the incidence of larger tumor volumes between the two groups were statistically significant, as indicated by asterisks in Figure 3. The volume of the largest tumor in the LFD group was 0.32 mm^3, while the volume of the largest tumor in the HAFD group was 2.59 mm^3. The number of tumors with volumes between 0.08 and 0.15 mm^3 was not significantly different in the LFD and HAFD groups.

A total of $n = 31$ tumors were detected in the HAFD group ($n = 8$) with an average of 3.9 ± 1.0 tumors per mouse, compared with a total of 10 tumors with an average of 1.2 ± 1.2 tumors per mouse in the LFD group ($n = 8$) ($p < 0.007$). The total tumor volume (sum of all tumor volumes) was 14.0 mm^3 with an average tumor volume per mouse of 0.5 ± 0.4 mm^3 in HAFD mice, compared with the total tumor volume of 2.0 mm^3 with an average tumor volume per mouse of 0.2 ± 0.1 mm^3 in LFD mice ($p < 0.016$).

Invasive tumors found in the *in vivo* MR images were correlated with histology. Figure 4 shows correlation of *in vivo* MRI, *ex vivo* MRI, and histological images of a 12-week-old SV40 mouse fed with HAFD. Two clearly visible masses are unambiguously identified as invasive cancers and they are marked with red arrows in both MR and H&E images. The *ex vivo* images provide an extra level of confidence for precise correlation.

Figure 5 compares histological H&E-stained images of the excised right inguinal mammary gland of LFD- and HAFD-fed mice at 12 weeks of age. Each image shown is a central slice containing the lymph node of the mammary gland. An experienced breast pathologist (J.M.) found several major differences between the LFD and HAFD SV40TAg mouse mammary glands. First, mammary glands from LFD mice showed highly visible brown fat containing numerous mitochondria, while HAFD mice show primarily mature, white fat, distinguished by a single lipid droplet in the adipocyte, seen in the insets of Figure 4A, B and indicated by black arrows. Second, mammary glands from HAFD mice showed more irregular and

dilated ducts compared with the LFD group, consistent with the MR images in Figure 2. Third, HAFD mice showed increased tumor invasiveness compared with LFD mice. Fourth, dilated blood vessels were seen in the gland of HAFD mice compared with the LFD group.

4 | DISCUSSION

The present MRI and histological study of the SV40TAg transgenic mouse model of humanTNBC unambiguously demonstrates that mice fed with high animal fat develop significantly more invasive mammary cancers, with a much larger overall mammary cancer burden. At 12 weeks of age, in the HAFD group the tumor incidence increased by a factor of 3 and the tumor burden increased by a factor of 7 compared with LFD group. The largest tumor volume was eight times greater in the HAFD group compared with the LFD group. Histology showed an increase in invasion in the HAFD-fed mice, indicative of aggressive cancers.

Figure 3 shows only modest (not statistically significant) differences between the number of small mammary cancers found in mice on the high fat versus low fat diets, but very large and significant differences between the number of larger cancers found in the two groups. This suggests that the primary effect of the HAFD in this mouse model is to promote the development of aggressive cancers, while effects on cancer incidence are less pronounced and likely dictated by the underlying TAg transgene.

SV40TAg mice on the HAFD did not gain significantly more weight compared with the mice on a regular diet, suggesting that critical changes affecting tumor growth occur in the mammary glands independently of systemic obesity.[15] It has been also suggested that an inflammatory state exists in animal models that is associated with excess systemic adiposity resulting from high fat diet consumption, which then promotes mammary cancer progression.[25–27] The connection between high fat diet/obesity and breast cancer has been attributed in part to adipose tissue dysfunction, which may occur locally within mammary fat pads,[28] even in the absence of systemic increased adiposity. In experiments parallel to those reported here, we found that 6 h fasting blood glucose in the HAFD-fed mice was only slightly elevated at 17 weeks of age, suggesting a lack of abnormal glucose homeostasis in the animals used at 12 weeks of age. It has been shown that HAFD diet increases adiposity, as seen in Figure 5B, epithelial cell proliferation, and the number of terminal ducts per mouse mammary gland in female mice.[28,29]

The MRI data reported here demonstrate that mammary glands can have localized increases in fat and overall parenchymal density although overall body weight is unchanged. Mammary gland histology shows that HAFD-fed mice have much less brown fat and increased white adipose tissue compared with LFD-fed mice. This is consistent with other work in this laboratory using chemical shift MRI, proton spectroscopy, and mass spectrometry (data not shown), demonstrating that fat content increases consistently and fat composition changes significantly in the HAFD group. In fact, our preliminary results show that the saturated fat fractions increased and the polyunsaturated fatty acid fractions decreased significantly in HAFD mice compared with LFD mice.[24] Overall, the HAFD diet

significantly changes mammary fat content without causing significant obesity, making it possible to study changes to mammary fat isolated from the systemic effects of obesity.

The HAFD results in abnormal mammary ductal development, seen here in HAFD-fed mice, as well as an incomplete lining of the epithelium surrounding the ductal lumen.[30] High fat-induced adiposity alters tight junction function and impairs the epithelial barrier.[31–34] Therefore, we hypothesize that the increased invasive cancer incidence observed in the HAFD-fed mice in our study may be in part due to increased propensity to invade through the ductal wall. Altered mammary fat content also secretes factors that promote cancer. Future studies are needed to define the mechanistic and metabolic links between HAFD, mammary gland biology, and the cancer incidence seen in the mouse model of TNBC.

Due to high spatial resolution and excellent soft tissue contrast, MRI, in contrast to CT or ultrasound, is an excellent tool for monitoring early *in situ* cancer and progression to invasive breast cancer. MRI reliably detects smaller tumors and allows accurate volume measurements. In addition, MRI allows evaluation of the surrounding parenchyma, including fat composition, as demonstrated by the present results. Although the present study involved only one scan per mouse, MRI could be used to serially image effects of diet and changes in diet on cancer initiation and progression over time.

Although functional images could improve the tumor delineation, we were able to accurately identify tumor boundaries from high resolution anatomical *in vivo* images in conjunction with *ex vivo* MR and histology images, as shown in Figure 4. We expect that *ex vivo* MRI will no longer be needed for MRI-histology correlations, as demonstrated here and in the previous study.[20] We selected 12 weeks of age for this initial study. This is the average age at which *in situ* cancers become invasive,[21] and therefore this is the best time to evaluate the effects of diet on tumor progression. Future longitudinal MRI studies will improve understanding of growth rates of both *in situ* and invasive mammary cancers and the transition from the *in situ* to the invasive phenotype in LFD and HAFD groups. Other dietary manipulations, e.g. a high fructose diet, can be used to model effects of similar diets in children through puberty to adulthood. Measurements of fat distribution and composition in the mammary gland and near invasive tumors using MRI will also improve our understanding of mammary gland fat biology and its role in driving breast cancer biology.

5 | CONCLUSION

The results reported here demonstrate that an HAFD significantly increases the number of aggressive cancers detected by MRI in a mouse model of human TNBC. We have also shown that diet-induced changes in mammary gland fat composition and distribution, which are associated with cancer progression, can be monitored by MRI. This work is the first step towards using MRI to improve the understanding of the effects of diet on mammary/breast cancer risk and guide development of methods that reduce risk.

Acknowledgments

Funding information

National Institutes of Health, Grant/Award Number: P30CA014599, R01-CA167785 and R01-CA133490; VPH-PRISM

This research is supported by grants from the National Institutes of Health (R01-CA133490, R01-CA167785, and P30CA014599), Florsheim Foundation, Segal Foundation, and a VPH-PRISM grant from the European Union.

Abbreviations used

DCIS	ductal carcinoma *in situ*
FOV	field of view
H&E	hematoxylin and eosin
HAFD	high animal fat diet
LFD	low fat diet
N_{EX}	number of excitations
RARE	rapid acquisition with relaxation enhancement
ROI	region of interest
SV40TAg mouse	C3(1)SV40 the simian virus 40 large T antigen (TAg) transgenic female mouse
TNBC	triple-negative breast cancer

References

1. DeSantis C, Siegel R, Bandi P, Jemal A. Breast cancer statistics, 2011. CA Cancer J Clin. 2011; 61(6):409–418. [PubMed: 21969133]
2. Hortobagyi GN, de la Garza Salazar J, Pritchard K, et al. The global breast cancer burden: Variations in epidemiology and survival. Clin Breast Cancer. 2005; 6(5):391–401. [PubMed: 16381622]
3. Yang XR, Chang-Claude J, Goode EL, et al. Associations of breast cancer risk factors with tumor subtypes: A pooled analysis from the breast cancer association consortium studies. J Natl Cancer Inst. 2011; 103(3):250–263. [PubMed: 21191117]
4. Hauner D, Janni W, Rack B, Hauner H. The effect of overweight and nutrition on prognosis in breast cancer. Dtsch Arztebl Int. 2011; 108(47):795–801. [PubMed: 22190993]
5. Kavanaugh C, Green JE. The use of genetically altered mice for breast cancer prevention studies. J Nutr. 2003; 133(7 Suppl):2404s–2409s. [PubMed: 12840216]
6. Sundaram S, Freemerman AJ, Johnson AR, et al. Role of HGF in obesity-associated tumorigenesis: C3(1)-TAg mice as a model for human basal-like breast cancer. Breast Cancer Res Treat. 2013; 142(3):489–503. [PubMed: 24218051]
7. Sundaram S, Le TL, Essaid L, et al. Weight loss reversed obesity-induced HGF/c-met pathway and basal-like breast cancer progression. Front Oncol. 2014; 4:175. [PubMed: 25072025]
8. Agurs-Collins T, Dunn BK, Browne D, Johnson KA, Lubet R. Epidemiology of health disparities in relation to the biology of estrogen receptor-negative breast cancer. Semin Oncol. 2010; 37(4):384–401. [PubMed: 20816508]
9. Chlebowski RT, Blackburn GL, Thomson CA, et al. Dietary fat reduction and breast cancer outcome: Interim efficacy results from the Women's intervention nutrition study. J Natl Cancer Inst. 2006; 98(24):1767–1776. [PubMed: 17179478]

10. Pierce JP. Diet and breast cancer prognosis: Making sense of the WHEL and WINS trials. Curr Opin Obstet Gynecol. 2009; 21(1):86–91. [PubMed: 19130632]
11. Green JE, Shibata MA, Yoshidome K, et al. The C3(1)/SV40 T-antigen transgenic mouse model of mammary cancer: Ductal epithelial cell targeting with multistage progression to carcinoma. Oncogene. 2000; 19(8):1020–1027. [PubMed: 10713685]
12. Maroulakou IG, Anver M, Garrett L, Green JE. Prostate and mammary adenocarcinoma in transgenic mice carrying a rat C3(1) simian virus 40 large tumor antigen fusion gene. Proc Natl Acad Sci U S A. 1994; 91(23):11236–11240. [PubMed: 7972041]
13. Herschkowitz JI, Simin K, Weigman VJ, et al. Identification of conserved gene expression features between murine mammary carcinoma models and human breast tumors. Genome Biol. 2007; 8(5):R76. [PubMed: 17493263]
14. Cleary MP, Grande JP, Maihle NJ. Effect of high fat diet on body weight and mammary tumor latency in MMTV-TGF-alpha mice. Int J Obes Relat Metab Disord. 2004; 28(8):956–962. [PubMed: 15254485]
15. Cowen S, McLaughlin SL, Hobbs G, et al. High-fat, high-calorie diet enhances mammary carcinogenesis and local inflammation in MMTV-PyMT mouse model of breast cancer. Cancer. 2015; 7(3):1125–1142.
16. Wirtzfeld LA, Ghoshal G, Rosado-Mendez IM, et al. Quantitative ultrasound comparison of MAT and 4T1 mammary tumors in mice and rats across multiple imaging systems. J Ultrasound Med. 2015; 34(8):1373–1383. [PubMed: 26206823]
17. Hipp E, Fan X, Jansen SA, et al. T_2* relaxation times of intraductal murine mammary cancer, invasive mammary cancer, and normal mammary gland. Med Phys. 2012; 39(3):1309–1313. [PubMed: 22380363]
18. Jansen SA, Conzen SD, Fan X, Markiewicz EJ, Newstead GM, Karczmar GS. Magnetic resonance imaging of the natural history of *in situ* mammary neo-plasia in transgenic mice: A pilot study. Breast Cancer Res. 2009; 11(5):R65. [PubMed: 19732414]
19. Jansen SA, Conzen SD, Fan X, et al. Detection of *in situ* mammary cancer in a transgenic mouse model: *in vitro* and *in vivo* MRI studies demonstrate his-topathologic correlation. Phys Med Biol. 2008; 53(19):5481–5493. [PubMed: 18780960]
20. Mustafi D, Zamora M, Fan X, et al. MRI accurately identifies early murine mammary cancers and reliably differentiates between *in situ* and invasive cancer: Correlation of MRI with histology. NMR Biomed. 2015; 28(9):1078–1086. [PubMed: 26152557]
21. Fan X, Mustafi D, Markiewicz E, et al. Mammary cancer initiation and progression studied with magnetic resonance imaging. Breast Cancer Res. 2014; 16(6):495. [PubMed: 25510596]
22. Volden PA, Wonder EL, Skor MN, et al. Chronic social isolation is associated with metabolic gene expression changes specific to mammary adipose tissue. Cancer Prev Res. 2013; 6(7):634–645.
23. Reeves PG, Nielsen FH, Fahey GC Jr. AIN-93 purified diets for laboratory rodents: Final report of the American Institute of Nutrition ad hoc writing committee on the reformulation of the AIN-76A rodent diet. J Nutr. 1993; 123(11):1939–1951. [PubMed: 8229312]
24. He, D., Mustafi, D., Fan, X., et al. MR spectroscopy shows that high fat diet changes composition and distribution of mammary gland fat in a transgenic mouse model of breast cancer. 25th Annual Meeting of the International Society of the Magnetic Resonance in Medicine; Honolulu, HI. 2017;
25. Duong MN, Cleret A, Matera EL, et al. Adipose cells promote resistance of breast cancer cells to trastuzumab-mediated antibody-dependent cellular cytotoxicity. Breast Cancer Res. 2015; 17:57. [PubMed: 25908175]
26. Iyengar NM, Zhou XK, Gucalp A, et al. Systemic correlates of white adipose tissue inflammation in early-stage breast cancer. Clin Cancer Res. 2016; 22(9):2283–2289. [PubMed: 26712688]
27. Stoll BA. Adiposity as a risk determinant for postmenopausal breast cancer. Int J Obes Relat Metab Disord. 2000; 24(5):527–533. [PubMed: 10849571]
28. Morris PG, Hudis CA, Giri D, et al. Inflammation and increased aromatase expression occur in the breast tissue of obese women with breast cancer. Cancer Prev Res. 2011; 4(7):1021–1029.
29. Montales MT, Melnyk SB, Simmen FA, Simmen RC. Maternal metabolic perturbations elicited by high-fat diet promote Wnt-1-induced mammary tumor risk in adult female offspring via long-term

effects on mammary and systemic phenotypes. Carcinogenesis. 2014; 35(9):2102–2112. [PubMed: 24832086]

30. Kamikawa A, Ichii O, Yamaji D, et al. Diet-induced obesity disrupts ductal development in the mammary glands of nonpregnant mice. Dev Dyn. 2009; 238(5):1092–1099. [PubMed: 19384959]
31. Khandekar MJ, Cohen P, Spiegelman BM. Molecular mechanisms of cancer development in obesity. Nat Rev Cancer. 2011; 11(12):886–895. [PubMed: 22113164]
32. Kundumani-Sridharan V, Dyukova E, Hansen DE 3rd, Rao GN. 12/15-lipoxygenase mediates high-fat diet-induced endothelial tight junction disruption and monocyte transmigration: A new role for 15(S)-hydroxyeicosatetraenoic acid in endothelial cell dysfunction. J Biol Chem. 2013; 288(22): 15830–15842. [PubMed: 23589307]
33. Le Drean G, Haure-Mirande V, Ferrier L, et al. Visceral adipose tissue and leptin increase colonic epithelial tight junction permeability via a RhoA- ROCK-dependent pathway. FASEB J. 2014; 28(3):1059–1070. [PubMed: 24243887]
34. Ma F, Ding X, Fan Y, et al. A CLDN1-negative phenotype predicts poor prognosis in triple-negative breast cancer. PLoS One. 2014; 9(11):e112765. [PubMed: 25393310]

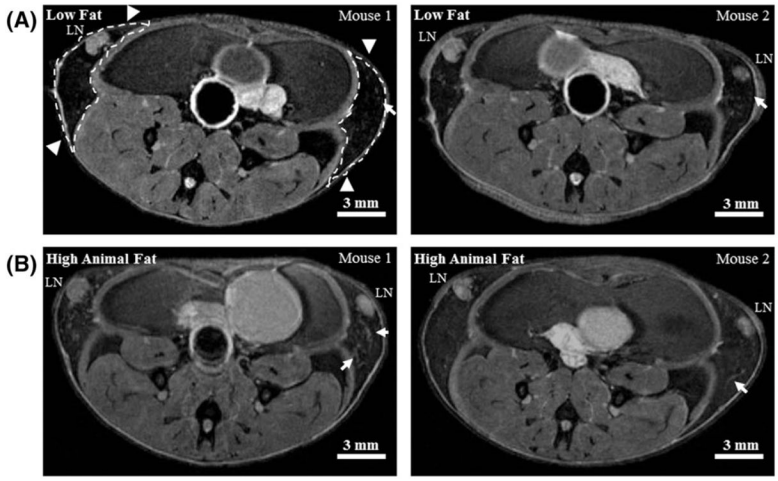

FIGURE 1.

In vivo MR images of low fat and high animal fat-fed SV40TAg mice. A, Two central slices of mouse inguinal glands from two separate LFD mice at 12 weeks of age. Inguinal glands are indicated by white dashed lines with arrowheads in the left image; LN—lymph node. B, The corresponding slices from two separate HAFD mice at 12 weeks of age. Images are shown to illustrate that high animal fat-fed mice have denser parenchyma, and thicker and irregular ducts, as indicated by white arrows, compared with LFD mice. Scale bars in all 2D T_2-weighted images are shown

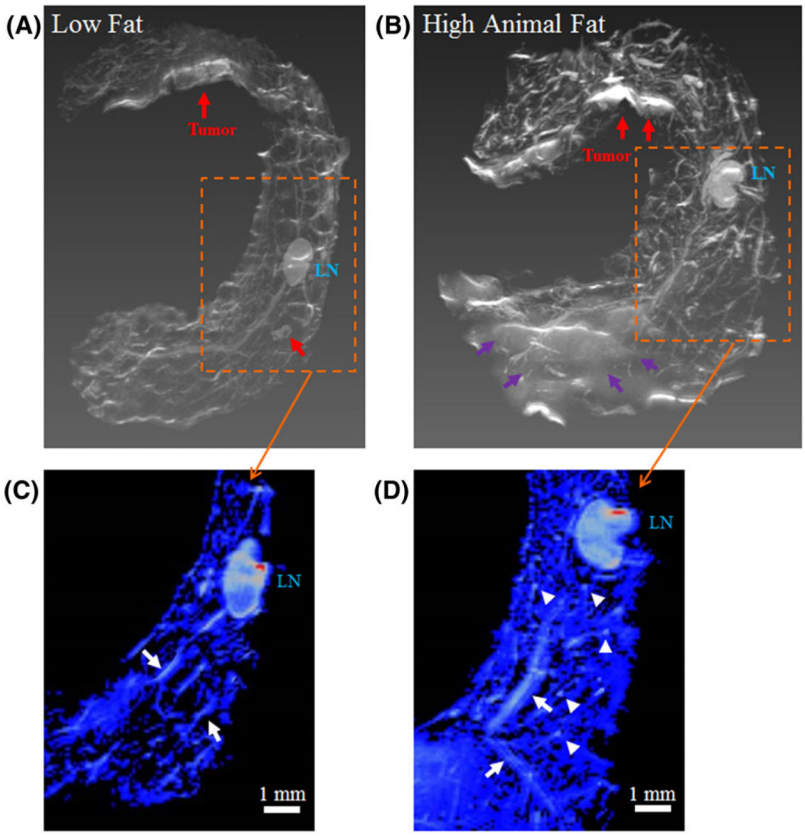

FIGURE 2.

Ex vivo MR images of mouse mammary glands of low fat and high animal fat-fed SV40TAg mice. 3D volume-rendered *ex vivo* MR images of the excised right inguinal glands of LFD and HAFD SV40TAg mice at 12 weeks of age are compared. A, B, Invasive cancers are labeled and indicated by red arrows in both sets of images. LN—lymph node. B, Purple arrows indicate the area that is only seen in HAFD mouse gland. This area was due to residual fat that failed to suppress fat completely although the fat-suppressed T_2-weighted protocol was used. C, D, *Ex vivo* MR images of LFD and HAFD mice are compared in the respective areas, indicated by boxes with dashed lines in A and B—in each image a central slice containing LN is shown here. Color images were produced with the same signal intensity of lymph nodes—Images are shown to illustrate that the HAFD mouse in D has denser parenchyma as indicated by blue color throughout the mammary gland compared with the LFD mouse in C. As indicated by the white arrows in D, thicker and more irregular ducts are seen in an HAFD mouse mammary gland compared with those in an LFD mouse, also indicated by white arrows in C. Also illustrated are more branching points as intense spots throughout the gland in the mammary gland of an HAFD mouse, as indicated by white arrowheads in D

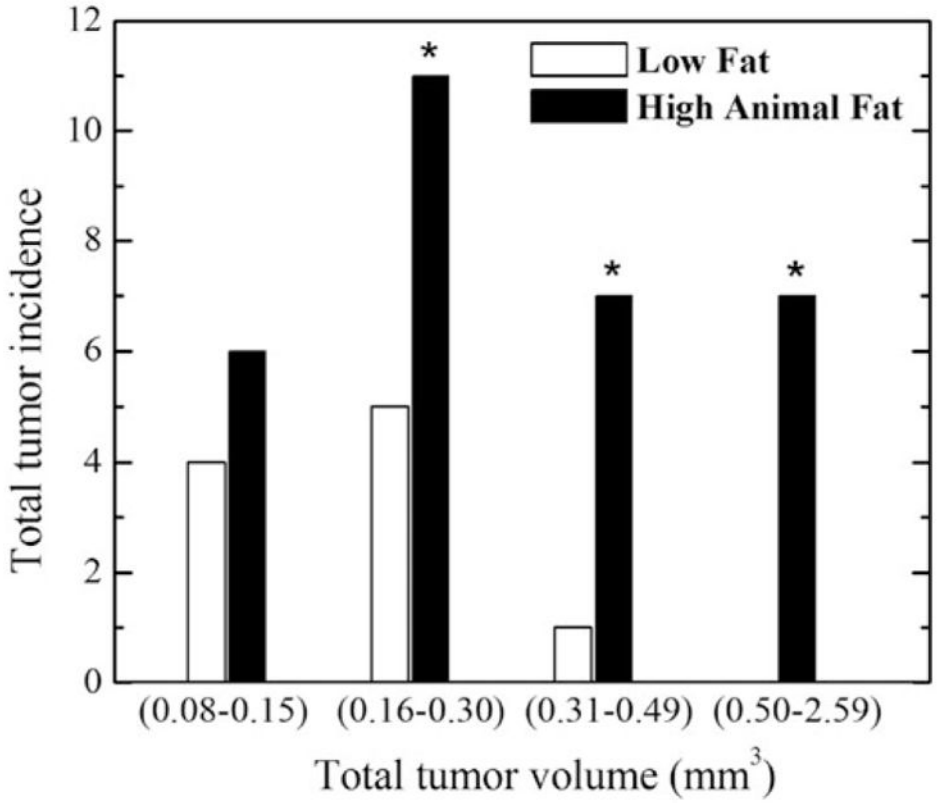

FIGURE 3.

Plot of tumor incidence as a function of tumor volume in low fat and high animal fat-fed SV40TAg mice. Tumor incidence and tumor volume in inguinal glands were measured from *in vivo* MRI in SV40TAg mice fed LFD or HAFD for 8 weeks, $n = 8$ 12-week-old mice in each group. The number of tumors for the smallest tumor volume subgroup of 0.08–0.15 mm^3 in the LFD group is not significantly different compared with the number of tumors in the HAFD group. However, the tumor incidences with larger tumor volumes of over 0.16 mm^3 are statistically significant, as indicated by asterisks in the plot

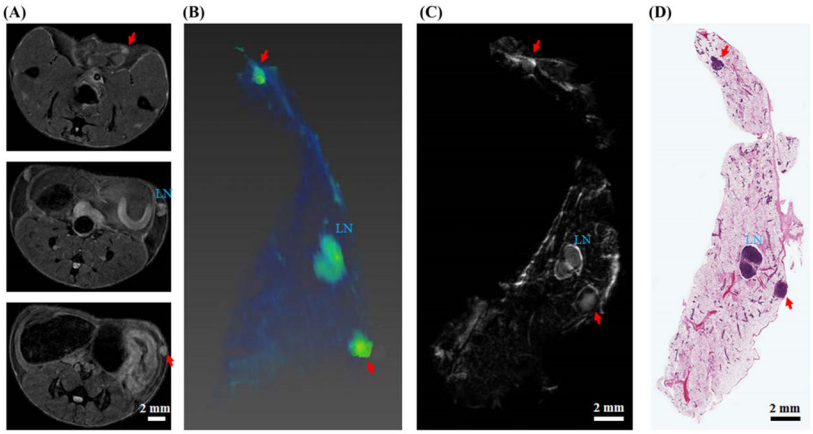

FIGURE 4.

Correlation of *in vivo* MR, *ex vivo* MR, and histological images of a 12-week-old SV40TAg mouse fed with HAFD. A, Three *in vivo* axial MR images; B, *in vivo* 3D volume-rendered image—only the right mammary gland is shown here. C, D, Comparison of an *ex vivo* MR image with an H&E image—in each case a central slice from the *ex vivo* MR and H&E images of the excised mammary gland is shown. The lymph node (LN) is labeled in each image; invasive cancers are indicated by two red arrows in *in vivo* MR, *ex vivo* MR, and H&E images

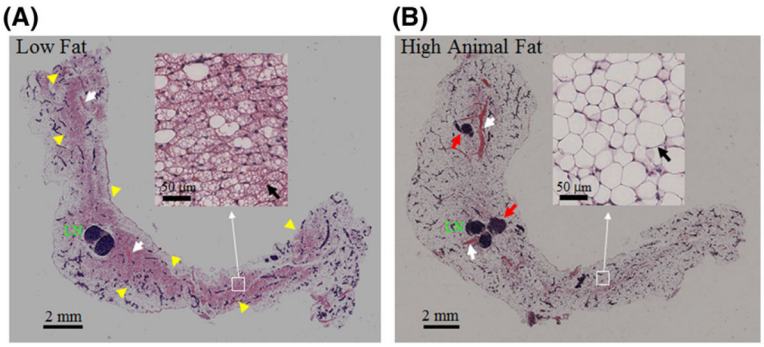

FIGURE 5.

Histological images of mouse mammary glands of low fat and high animal fat-fed SV40TAg mice. H&E-stained images of the excised right inguinal glands of LFD and HAFD SV40TAg mice at 12 weeks of age are compared. In each image a central slice of the mammary gland containing the lymph node (LN) is shown. In B two tumors are seen, as indicated by red arrows. Blood vessels in both images are indicated by white arrows—dilated blood vessels are seen in HAFD mouse mammary gland. Highly visible brown fat throughout the gland in the LFD mouse is indicated by yellow arrowheads in A. Insets—areas corresponding to white boxes as indicated—show H&E-stained images with higher magnification. Highly visible brown fat, characterized by multiloculated adipocytes, predominates in the LFD mouse mammary gland. In contrast, the HAFD mouse mammary gland shows primarily mature fat, which is distinguished by the single lipid droplet in the adipocyte. These are indicated by black arrows in both images in insets

TABLE 1

Selected nutrients and ingredients in low fat and high animal fat diets

Components	**LFD**	**HAFD**
Nutrients	% by weight	% by weight
Protein	17.7	17.7
Carbohydrate	60.1	34.9
Fat	7.2	35.2
Ingredients	g/kg	g/kg
Casein	200	200
L-cystine	3	3
Corn starch	398	117
Maltodextrin	132	132
Sucrose	100	100
Soybean oil	70	70
Lard	- -	280
Cellulose	50	50
Mineral mix	35	35
Vitamin mix	10	10
Choline bitartrate	2.5	2.5
Antioxidant	0.014	0.014
Food coloring	—	0.1